J Electr Eng Technol.2015; 10(2): 443-451
http://dx.doi.org/10.5370/JEET.2015.10.2.443

ISSN(Print) 1975-0102
ISSN(Online) 2093-7423

Estimating Stability of MTDC Systems with Different Control Strategy

Thai-Thanh Nguyen*, Ho-Ik Son* and Hak-Man Kim†

Abstract – The stability of a multi-terminal direct current (MTDC) system is often influenced by its control strategy. To improve the stability of the MTDC system, the control strategy of the MTDC system must be appropriately adopted. This paper deals with estimating stability of a MTDC system based on the line-commutated converter based high voltage direct current (LCC HVDC) system with an inverter with constant extinction angle (CEA) control or a rectifier with constant ignition angle (CIA) control. In order to evaluate effects of two control strategies on stability, a MTDC system is tested on two conditions: initialization and changing DC power transfer. In order to compare the stability effects of the MTDC system according to each control strategy, a mathematical MTDC model is analyzed in frequency domain and time domain. In addition, Bode stability criterion and transient response are carried out to estimate its stability.

Keywords: Multi-terminal Direct Current, Control strategy, Stability of MTDC system, Line-commutated converter (LCC) HVDC system.

1. Introduction

A multi-terminal direct current (MTDC) system had been researched since early 1963 [1]. With the benefits of the MTDC system such as flexibility in energy exchange and economics, extending HVDC systems into the MTDC system became an technical issue [2, 3]. A MTDC system can be classified into three categories according to composed three-phase converters: a MTDC system based on the voltage source converter (VSC-MTDC), a MTDC system based on the line-commutated converter (LCC-MTDC), and a hybrid MTDC system based on both VSC and LCC converters. The MTDC system based on VSC HVDC technology is the most investigated owing to its advantages such as operation in AC grids with low short-circuit capacity, fast transient response, and black start capability. However, the disadvantages of this configuration are the high investment cost, high power losses, and low power capability. Nowadays, the development of modular multilevel converters (MMC) is improving the power capability of VSC HVDC with reduced power losses. Thus, a MTDC system based on MMC HVDC will be more attractive with respect to reliability and fault handing. By comparison, a MTDC system based LCC HVDC technology still remains the dominant technology for bulk power transmission over long distances owing to low investment cost and much high maximum power transfer capacities. A hybrid MTDC system has combined advantages of both VSC and LCC HVDC technologies. It is estimated that each type of the MTDC system plays an important role in the HVDC network connecting offshore and onshore grids. That is, the VSC-MTDC system can be a potential solution for integration offshore wind farms as well as connection offshore wind farms to the onshore grids [4-9], the hybrid MTDC system with the unidirectional power transfer is suitable for connection offshore to onshore grids [10, 11], and the LCC-MTDC system is often placed on onshore grid [12-14]. Especially, the LCC-MTDC system has been developed in few projects, such as the Quebec-New England HVDC, the North-East Agra link, and the Northwest China [13-15].

Meanwhile, control strategy plays an important role in the LCC-MTDC system due to interaction between AC and DC systems. In 1980, several types of control strategies of LCC-MTDC systems were demonstrated and compared with different operating conditions but they didn't deal with clearly the preferable control strategy for the LCC-MTDC system [16, 17]. Therefore, the main purpose of this study is to propose the suitable control strategy for the LCC-MTDC system.

Power system stability is the property of an electric power system that enables it to remain in a state of operating equilibrium under normal operating conditions and to regain an acceptable state of equilibrium after being subjected to a disturbance [18]. As a result, in this study, initialization and power change conditions are applied to estimate stability of the LCC-MTDC system according to control strategies. LCC-MTDC system stability is estimated by using time domain analysis or frequency domain analysis of its mathematical model. Several methods were used to estimate stability of the LCC-MTDC system. Stability of the LCC-MTDC system was estimated by analysis its mathematical model in frequency domain [19, 20]. In 1980, the LCC-MTDC system with 3-terminals and 7-terminals were modeled in a transient stability

† Corresponding Author: Dept. of Electrical Engineering, Incheon National University, Incheon, Korea (hmkim@incheon.ac.kr)
* Dept. of Electrical Engineering, Incheon National University, Incheon, Korea. ({ntthanh, shi0617}@incheon.ac.kr)
Received: September 20, 2014; Accepted: January 19, 2015

program, but only one type of control strategy was applied to the LCC-MTDC system [21]. The stability of the LCC-MTDC system was also estimated by digital simulation [22] or eigenvalues analysis [23]. This paper analyzes stability of the LCC-MTDC system with its mathematical model.

In this paper, firstly, a MTDC system based on LCC-HVDC with 3-terminals shown in Fig. 1 is modeled in PSCAD/EMTDC under two types of control strategies: CEA-type control based on constant extinction angle (CEA) control on inverter 1 as a receiving converter and CIA-type control based on constant ignition angle (CIA) control on a rectifier as a sending converter. Secondly, a mathematical MTDC model is developed based on the impulse model. MATLAB/SIMULINK program is used for modeling mathematical MTDC system with different types of control strategies. Bode stability criterion is used to estimate the stability of the MTDC system in frequency domain. The bandwidth of the close-loop system is also carried out to evaluate the transient response of the system in time domain. Finally, the MTDC system is evaluated on two operation conditions such as initialization and changing DC power transfer.

2. MTDC Modeling

This paper considers a MTDC system with 3-terminals connected in parallel as shown in Fig. 1 as mentioned before. The AC sides of the MTDC system include AC supply networks, AC filters, and transformers on each AC side of converters. AC supply networks are modeled by voltage sources connected in series with a thevenin equivalent impedance of the AC system [24]. The strength of the AC system illustrated by the short circuit ratio (SCR) has a significant impact on AC/DC system interactions. AC filters such as single tuned and high pass filters are used to eliminate harmonic voltage and current generated by converters. Additionally, they also provide the reactive power to converters [25]. Transformers are added on both a rectifier and inverter sides for the purpose of providing the appropriate voltage level to valve bridges.

The DC side of the MTDC system is composed of DC smoothing reactors and DC cables with the length of 100 km for each line. The cables are based on the Frequency Dependent (Phase) model in PSCAD/EMTDC to study the transient behavior of the cable [26].

Converters are modeled by the 6-pulse Graetz converter bridge in PSCAD / EMTDC. Thyristor valves are used as an ideal switch parallel with a snubber circuit for each thyristor.

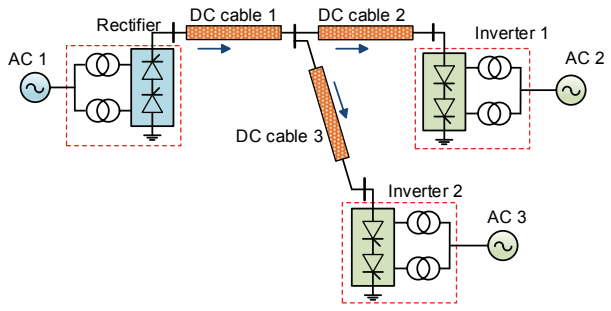

Fig. 1. MTDC System

3. Control Strategy of MTDC System

Firing angle (α), extinction angle (γ), and direct current at each converter are used as input signals to control systems such as constant current (CC), CEA or CIA. Nevertheless, each converter has different type of the control mode depending on control strategy. Fig. 2 shows the V-I characteristics of each control strategy. In CEA-type control, the rectifier and inverter 2 have CC control. Besides, inverter 1 has CEA and CC control. Under normal condition, the rectifier and inverter 2 operate at the current control mode and inverter 1 operates at the voltage control mode. In this type, inverter 1 is the voltage setting terminal. By comparison, in CIA-type control, the rectifier has CIA and CC control while inverters 1 and 2 have CC control. At the normal condition, the rectifier is on the CIA control mode to determine system voltage.

In addition, significantly decreasing voltage at the inverter terminal may lead to commutation failures and cause the collapse of DC voltage. Therefore, voltage dependent current order limit (VDCOL) is used to reduce the allowable maximum direct current when voltage drops below the predetermined value [18]. VDCOL is not shown in Fig. 2 for the sake of simplicity.

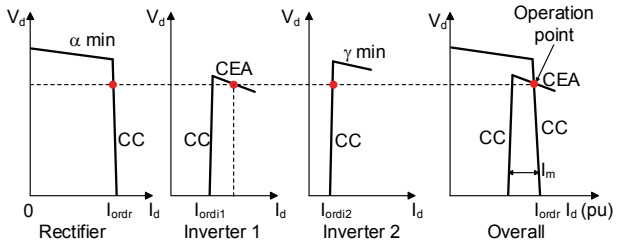

(a) CEA-type control

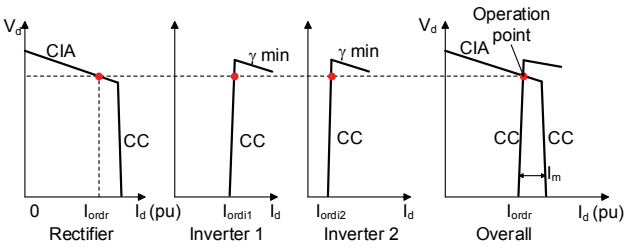

(b) CIA-type control

Fig. 2. V-I characteristics with different control strategy

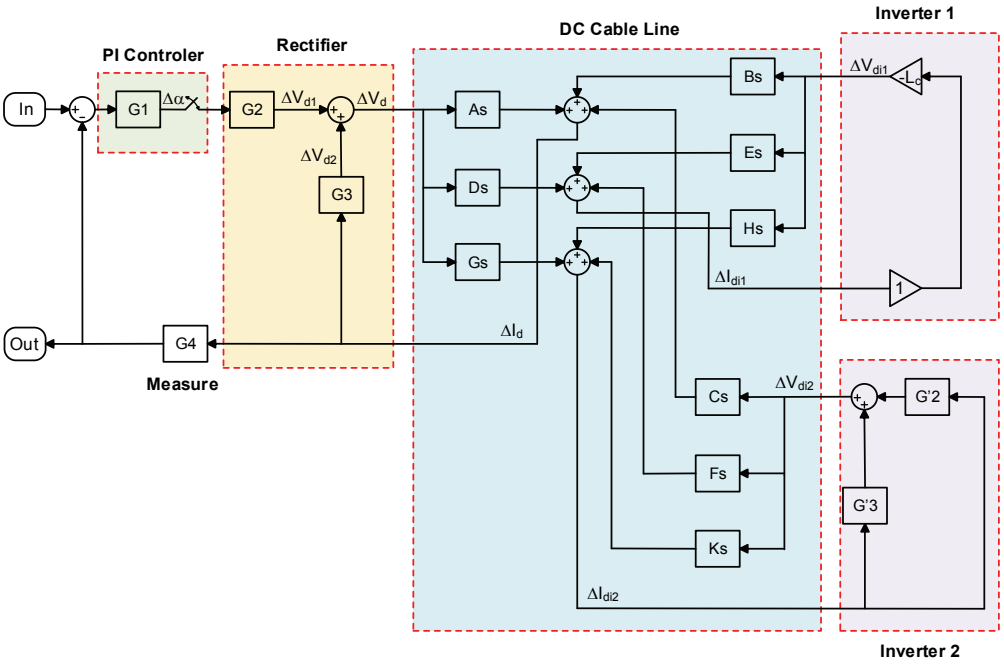

Fig. 3. Block diagram of MTDC system in CEA-type control

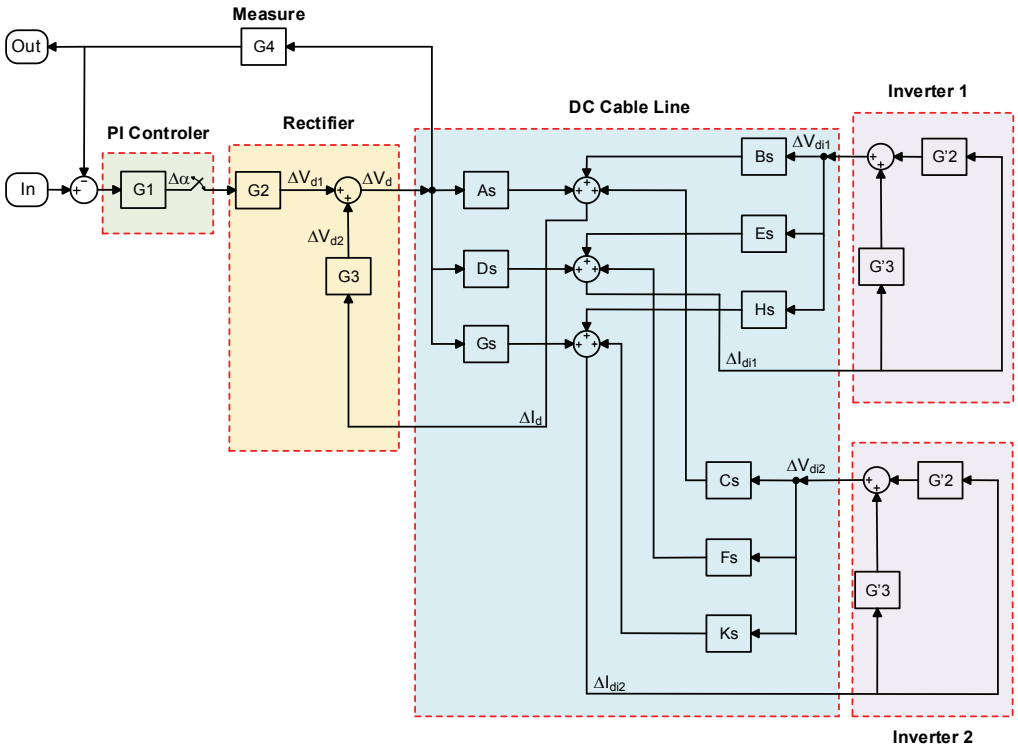

Fig. 4. Block diagram of MTDC system in CIA-type control

4. Mathematical MTDC Model of Control System

In this section, a MTDC system considering two types of control strategies is modeled mathematically to estimate its stability. The block diagrams of the close-loop control system in CEA-type control and CIA-type control are shown in Figs. 3 and 4, respectively. The difference between CEA-type control and CIA-type control is the feedback of the close-loop control system. That is, CEA-type control has rectifier current feedback to remain constant current under the normal condition and CIA-type control has rectifier voltage feedback to remain constant voltage. Both types of control strategies are implemented by proportional - integral (PI) control which is represented by transfer function *G1* in Figs. 3 and 4.

4.1 Rectifier model

Output voltage of the rectifier is influenced by change in firing angle and voltage drop due to commutation inductance of AC source. In [27], the rectifier was considered as an ideal sampler. If a small variation $\Delta\alpha$ of firing angle is considered with constant output current, the increment in output voltage will be consisted of two pulses in each firing period. Fig. 5 (a) shows the positive and negative $\Delta\alpha$.

The change of output voltage with $\Delta\alpha$ is determined by area ΔA_1 and ΔA_2 as shown in Fig. 5 (a). Area ΔA_1 equals to area ΔA_2 because of constant output current. These areas are given by:

$$\Delta A_1 = \frac{1}{2} V_{d0} T_s \sin\alpha^0 \Delta\alpha \quad (1)$$

$$\Delta A_2 = \Delta A_1 \quad (2)$$

where α^0 is the normal firing angle, T_s is the sampling period, and V_{d0} is the ideal no-load voltage.

If a small variation ΔI_d is considered with constant firing angle, the change of output voltage is represented by area ΔA in Fig. 5 (b).

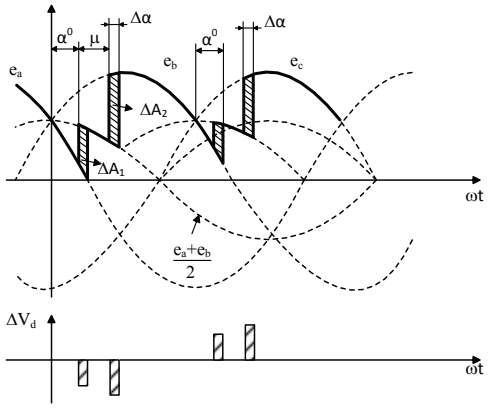

(a) Small variation of firing angle

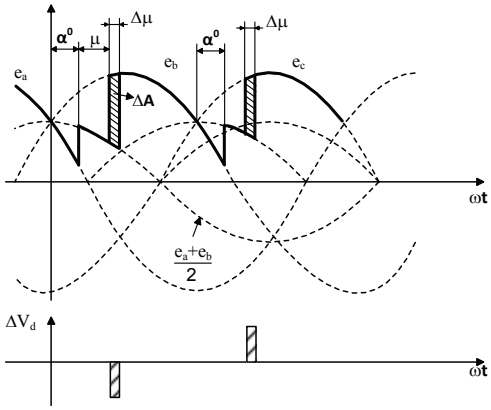

(b) Small variation of output current

Fig. 5. Incremental output voltage

$$\Delta A = L_C \Delta I_d \quad (3)$$

where L_C is commutating inductance per phase.

The block diagram of the rectifier model is shown in Fig. 3. The increment voltage ΔV_d is given by:

$$\Delta V_d = G2(s)\Delta\alpha + G3(s)\Delta I_d \quad (4)$$

The transfer function $G2(s)$ given by Eq. (5) shows the output voltage of the rectifier with $\Delta\alpha$. It means that the incremental rectifier voltage is made of two identical impulses which shown in Fig. 5(a). The first impulse occurred at instant firing angle, and the second impulse is delayed by commutation time, $T_\mu = \frac{\mu}{\omega}$. The transfer function $G3(s)$ represents the incremental output voltage with ΔI_d. This period can be considered as a single pulse delayed by commutation time, T_μ with respect to the instant firing angle.

$$G2(s) = -\frac{1}{2} V_{d0} T_s \sin\alpha^0 \{1 + e^{-sT_\mu}\} \quad (5)$$

$$G3(s) = -L_c e^{-sT_\mu} \quad (6)$$

4.2 Inverter model

As shown in Fig. 3, the block diagram of inverters 1 and 2 is different owing to the control mode under the steady-state condition. That is, inverter 1 is operated at the CEA mode and inverter 2 is operated at the CC mode. To deal with the CEA control mode of the inverter, this paper uses its lumped block diagram proposed in [27]. Beside, inverter 2 has the CC control mode, and its block diagram is similar to the rectifier model with the transfer function $G'2$ and $G'3$ represented by following equations:

$$G'2(s) = -\frac{1}{2} V'_{d0} T_s \sin\beta \{1 + e^{-sT'_\mu}\} \quad (7)$$

$$G'3(s) = -L'_c e^{-sT'_\mu} \quad (8)$$

where $\beta = \pi - \alpha^0$ is ignition advance angle.

4.3 DC line

The DC cable line can be replaced by the T or Π model, which includes series and shunt resistance, inductance, and capacitance of the line. However, for a straightforward 3-terminals MTDC system, the DC cable line is represented by the series element only [19]. According to [21], the shunt capacitance of the line can be neglected due to its insignificant effect on transient stability. As results, in this paper, the DC line is replaced by a lumped-parameter R-L element which shown in Fig. 6. Smoothing inductance is

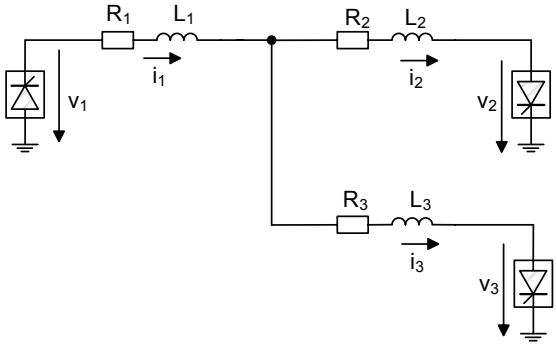

Fig. 6. DC line T-section

also included in the line parameter. By using Kirchhoff's circuit laws to solve the circuit shown in Fig. 6, the circuit equation matrix of the DC cable line can be obtained by:

$$\begin{bmatrix} i_1 \\ i_2 \\ i_3 \end{bmatrix} = \begin{bmatrix} A & B & C \\ D & E & F \\ G & H & K \end{bmatrix} \begin{bmatrix} v_1 \\ v_2 \\ v_3 \end{bmatrix} \tag{9}$$

Therefore, the admittance matrix in term of the Laplace transfer function shown in Figs. 3 and 4 is given by the following:

$$\begin{bmatrix} I_1 \\ I_2 \\ I_3 \end{bmatrix} = \begin{bmatrix} As & Bs & Cs \\ Ds & Es & Fs \\ Gs & Hs & Ks \end{bmatrix} \begin{bmatrix} V_1 \\ V_2 \\ V_3 \end{bmatrix} \tag{10}$$

where

$$As = \frac{Z_2 + Z_3}{Z_1Z_2 + Z_1Z_3 + Z_2Z_3}$$

$$Bs = \frac{-Z_3}{Z_1Z_2 + Z_1Z_3 + Z_2Z_3}$$

$$Cs = \frac{-Z_2}{Z_1Z_2 + Z_1Z_3 + Z_2Z_3}$$

$$Ds = \frac{Z_3}{Z_1Z_2 + Z_1Z_3 + Z_2Z_3}$$

$$Es = \frac{-(Z_1 + Z_3)}{Z_1Z_2 + Z_1Z_3 + Z_2Z_3}$$

$$Fs = \frac{Z_1}{Z_1Z_2 + Z_1Z_3 + Z_2Z_3}$$

$$Gs = \frac{Z_2}{Z_1Z_2 + Z_1Z_3 + Z_2Z_3}$$

$$Hs = \frac{Z_1}{Z_1Z_2 + Z_1Z_3 + Z_2Z_3}$$

$$Ks = \frac{-(Z_1 + Z_2)}{Z_1Z_2 + Z_1Z_3 + Z_2Z_3}$$

$$Z_1 = R_1 + sL_1\,;\quad Z_2 = R_2 + sL_2; Z_3 = R_3 + sL_3$$

4.4 The transfer function of control system

Block diagrams of the control system of the MTDC system shown in Figs. 3 and 4 are built in MATLAB / SIMULINK. The steady-space models of *G2* and *G'2* include the internal time delays that cannot be converted to transfer function form in Simulink models. As a consequence, the "*pade*" function that represents a Padé approximant is applied to approximate these transfer function. The open-loop transfer function of the MTDC system is carried out by "*linmod*" function.

5. Simulation Results

5.1 Calculated frequency response for MTDC system

Fig. 7 shows the frequency response of the MTDC system in term of the Bode diagram. Gain margin and phase margin of the open-loop control system also are shown in the figure. In order to maintain the stable close-

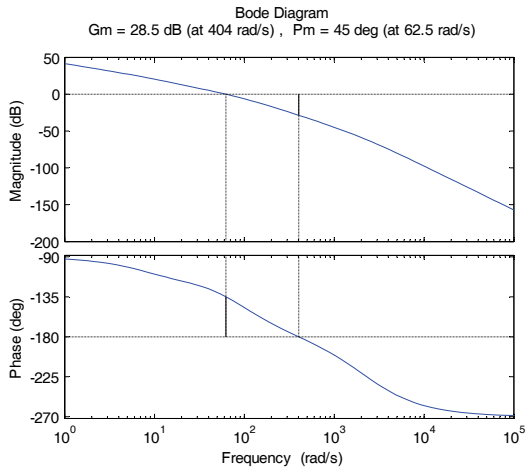

(a) CEA-type control

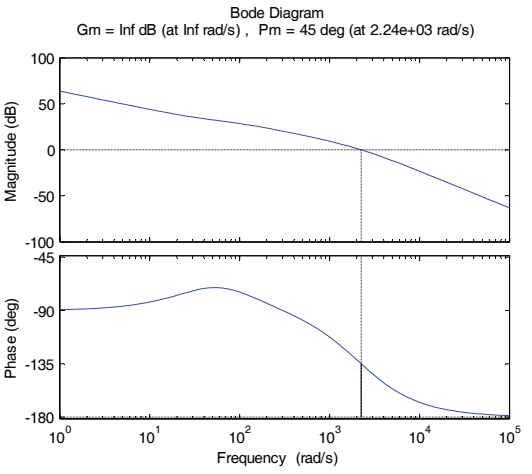

(b) CIA-type control

Fig. 7. Bode diagram for open-loop control system

loop response, PI parameter was chosen to satisfy as in (11) and (12) [28].

$$Gain\,margin \geq 6dB \tag{11}$$

$$30° \leq Phase\,margin \leq 60° \tag{12}$$

As shown in Fig. 7, the gain margins of the open-loop MTDC system in CEA-type control and CIA-type control are 28.5 dB and infinite, respectively. The phase margin is 45° for both types of control. Obviously, the system with large gain margin is more stable than one with smaller gain margin by same phase margin [29]. As a result, the MTDC system under CIA-type control is more stable than that under CEA-type control. Additionally, the bandwidth of the control system gives indication on the transient-response properties in the time domain with larger bandwidths corresponds to faster rise time. In this paper, the bandwidths of the MTDC system under CEA-type control and CIA-type control are 16.509 Hz and 573 Hz, respectively. Thus, the MTDC system under CIA-type control has a faster rise time than CEA-type control.

5.2 Operation characteristic of MTDC system

In order to estimate the stability of the MTDC system, the simulation is carried out on initialization and changing DC power transfer conditions.

Fig. 8 shows the system characteristics under the initialization condition with two types of control strategies. In this figure, direct current, direct voltage, and firing angle are illustrated. The current orders at inverters 1 and 2 are 0.7 and 0.3 pu, respectively. The transient response of direct current at the initialization is shown in Figs. 8 (a) and (b), where it can be seen that the rise time of direct current in CEA-type control with 0.48 s is about fourth times higher than that in CIA-type control. This trend is similar to the direct voltage and firing angle at the converter under two types of control strategies. Furthermore, the fluctuations of direct voltage and current under initialization process in CEA-type control are larger than CIA-type control. In other words, the MTDC system under CIA-type control is more stable than CEA-type control.

The characteristics of the MTDC system under changing DC power transfer are shown in Fig. 9. DC power transfer from rectifier to inverters 1 and 2 is changed by adjusting current order to each converter. Fig. 9 shows that transient response of the MTDC system under CIA-type control is faster than CEA-type control, and the MTDC system under CIA-type control is more stable than CEA-type control. Additionally, when the current order to inverters 1 and 2 is adjusted at 2 s, the transient response of current in CIA-type control is nearly immediate. By comparison, the

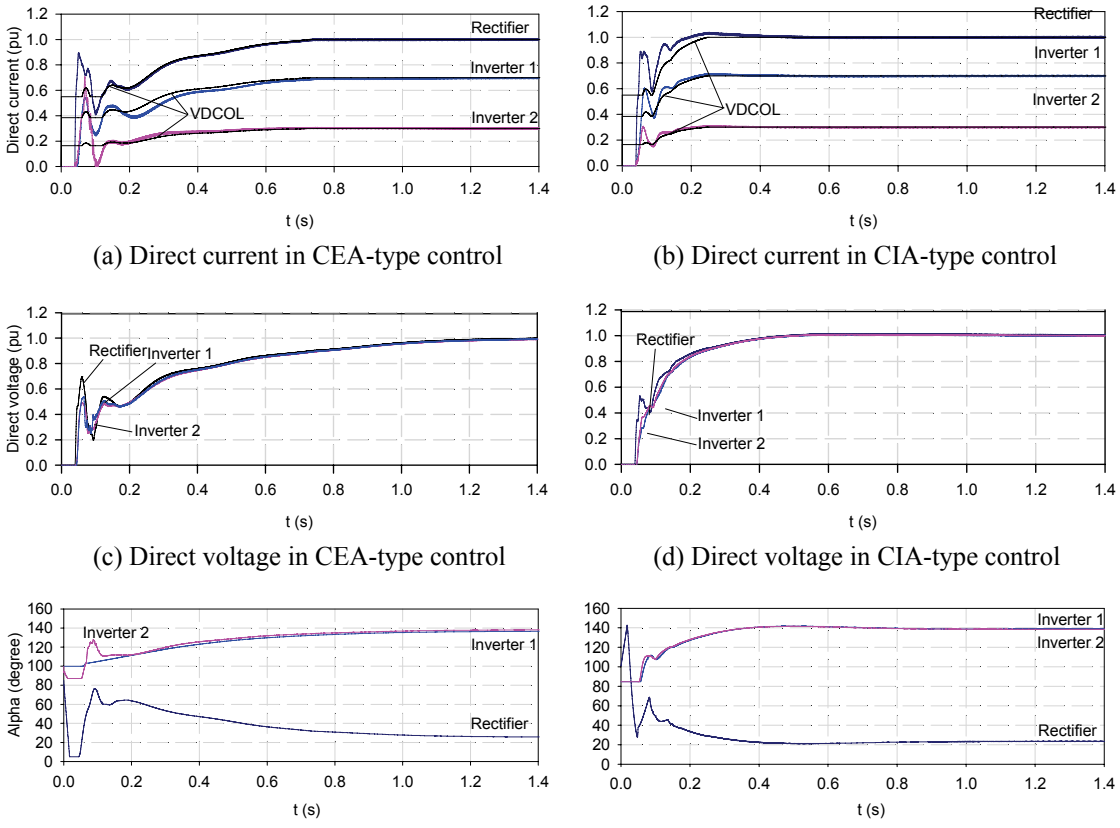

(a) Direct current in CEA-type control

(b) Direct current in CIA-type control

(c) Direct voltage in CEA-type control

(d) Direct voltage in CIA-type control

(e) Firing angle in CEA-type control

(f) Firing angle in CIA-type control

Fig. 8. Initialization of MTDC system

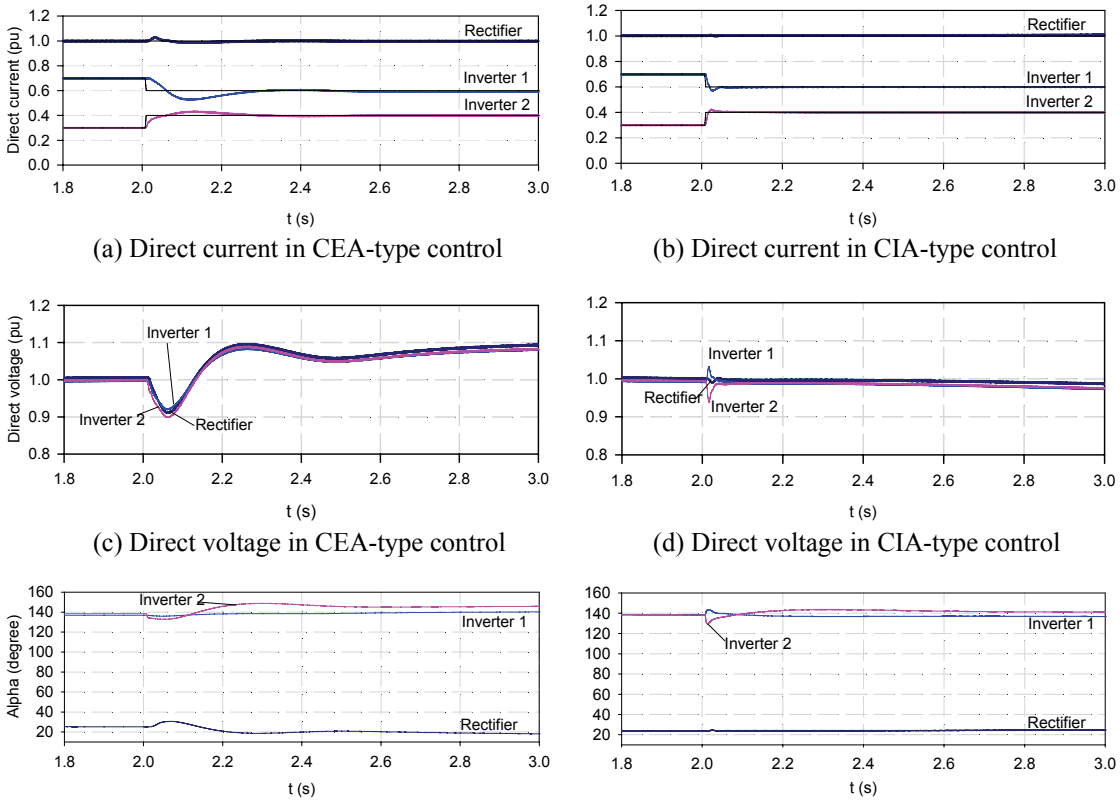

(a) Direct current in CEA-type control

(b) Direct current in CIA-type control

(c) Direct voltage in CEA-type control

(d) Direct voltage in CIA-type control

(e) Firing angle in CEA-type control

(f) Firing angle in CIA-type control

Fig. 9. Changing DC power transfer

transient response of direct current in CEA-type control is slower than CIA-type control. Besides, after changing DC power transfer, fluctuation of direct voltage in CEA-type control is bigger than CIA-type control. In CEA-type control, direct voltage reached to 1.1 pu at the new stable operating point while direct voltage at converter was remained unchanged at 1 pu.

6. Conclusion

The VSC-MTDC system and the hybrid MTDC system become more attractive. However, with their lower power capability and higher investment cost compared to the LCC-MTDC system, it is anticipated that the LCC-MTDC still plays an important position in the future grids, such as integration onshore grids over long distances and bulk power transmission. This paper dealt with the proper control strategy for the LCC-MTDC system with high stability and fast response.

Two types of control strategies for the LCC-MTDC system were analyzed using a LCC-MTDC system modeled in PSCAD / EMTDC program as well as MATLAB / SIMULINK under different operation conditions. The simulations results showed that the LCC-MTDC system based on CIA-type control is more stable and has faster response than CEA-type control. It can be explained as follows;

a) Since inverter 1 plays a role of voltage setting terminal in CEA-type control, it cannot control the current at its terminal in case of system disturbance or load change. However, in CIA-type control, all inverters can control current at its terminals.
b) In addition, system voltage can be controlled by a rectifier with largest power at its terminal. Thus, the LCC-MTDC system based on CIA-type control is more stable and faster response than other ones.

In case of a LCC-MTDC system with multiple rectifiers, additionally, we suggest that a rectifier terminal with the largest power should be the voltage setting terminal to operate stably the LCC-MTDC system.

Appendix

The parameters of MTDC system are as follows.

Table 1. Parameters of MTDC system

Parameter	Rectifier	Inverter 1	Inverter 2
AC frequency [Hz]	60	60	60
AC voltage [kV]	345	345	345
SCR	3∠-85º	3∠-85º	3∠-85º
DC voltage [kV]	500	500	500
DC power [MW]	1000	700	300
Inductance of AC source [H]	0.005	0.005	0.005

- Cable parameters:

- *Length of DC cable = 100 km*
- *Resistance of cable r = 0.07 Ω/km*
- *Inductance of cable l = 0.0024 H/km*

- Converter parameters:

- *Firing angle $\alpha = 24°$*
- *Ignition advance angle $\beta = 24°$*
- *Overlap angle $\mu = 20°$*
- *Smoothing inductance L = 0.5 H*

References

[1] U. Lamm, E. Uhlmann, and P. Danfors, "Some Aspects of Tapping HVDC Transmission Systems," Direct Current, vol. 8, no. 5, pp. 124-129, May 1963.

[2] W. F. Long, J. Reeve, J. R. McNichol, M. S. Holland, J. P. Taisne, J. Lemay, and D. J Lorden, "Application Aspects of Multiterminal DC Power Transmission," IEEE Trans. Power Delivery, vol. 5, no 4, pp. 2084-2098, 1990.

[3] P. C. S. Krishnayya, S. Lefebvre, V. K. Sood, and N. J. Balu, "Simulator Study of Multiterminal HVDC System with Small Parallel Tap and Weak AC Systems," IEEE Trans. Power Apparatus and Systems, vol. PAS-103, no. 10, pp. 3125-3132, Oct. 1984.

[4] Zhu Jiebei, J. M. Guerrero, W. Hung, C. D. Booth, and G. P. Adam, "Generic Inertia Emulation Controller for Multi-Terminal Voltage-Source-Converter High Voltage Direct Current Systems," IET Renewable Power Generation, vol. 8, no. 7, pp. 740-748, Sep. 2014.

[5] J. Beerten, S. Cole, and R. Belmans, "Modeling of Multi-Terminal VSC HVDC Systems With Distributed DC Voltage Control," IEEE Trans. Power Systems, vol. 29, no. 1, pp. 34-42, Jan. 2014.

[6] R. T. Pinto, P. Bauer, S. F. Rodrigues, E. J. Wiggelinkhuizen, J. Pierik, and B. Ferreira, "A Novel Distributed Direct-Voltage Control Strategy for Grid Integration of Offshore Wind Energy Systems Through MTDC Network," IEEE Trans. Industrial Electronics, vol. 60, no. 6, pp. 2429-2411, June 2013.

[7] Wang Wenyuan and M. Barnes, "Power Flow Algorithms for Multi-Terminal VSC-HVDC with Droop Control," IEEE Trans. Power Systems, vol. 29, no. 4, pp. 1721-1730, July, 2014.

[8] V. Akhmatov, M. Callavik, C. M. Franck, S. E. Rye, T. Ahndorf, M. K. Bucher, H. Muller, F. Schettler, and R. Wiget, "Technical Guidelines and Prestandardization Work for First HVDC Grids," IEEE Trans. Power Delivery, vol. 29, no. 1, pp. 327-335, Feb. 2014.

[9] Wang Wenyuan, A. Beddard, M. Barnes, and O. Marjanovic, "Analysis of Active Power Control for VSC-HVDC," IEEE Trans. Power Delivery, vol. 29, no. 4, pp. 1978-1988, Aug. 2014.

[10] Li Chenghao, Zhan Peng, Wen Jinyu, Yao Meiqi, Li Naihu, and Lee Wei-Jen, "Offshore Wind Farm Integration and Frequency Support Control Utilizing Hybrid Multiterminal HVDC Transmission," IEEE Trans. Industry Applications, vol. 50, no. 4, pp. 2788-2707, July-Aug. 2014.

[11] Chen Xia, Sun Haishun, Yuan Xufeng, Wen Jinyu, Li Naihu, Yao Liangzhong, and Lee Wei-Jen, "Integrating Wind Farm to The Grid Using Hybrid Multi-Terminal HVDC Technology," Proc. of IEEE Industrial and Commerical Power Systems Technical Conference (I&CPS), pp. 1-6, May 2010.

[12] Weixing Lin, Jinyu Wen, Jun Liang, Shijie Cheng, Meiqi Yao, and Naihu Li, "A Three-Terminal HVDC System to Bundle Wind Farms With Conventional Power Plants," IEEE Trans. Power Systems, vol. 28, no. 3, pp. 2292-2300, Aug. 2013.

[13] http://new.abb.com/systems/hvdc/references/quebec-new-england

[14] http://new.abb.com/systems/hvdc/references/north-east-agra

[15] Chen Xia, Lin Weixing, Sun Haishun, Wen Jinyu, Li Naihu, and Yao Liangzhong, "LCC Based MTDC for Grid Integration of Large Onshore Wind Farms in Northwest China," Proc. of IEEE Power and Energy Society General Meeting, pp. 1-10, July 2011.

[16] J. Reeve, "Multiterminal HVDC Power System," IEEE Trans. Power Apparatus and Systems, vol. PAS-99, no. 2, pp. 729-737, Mar./Apr. 1980.

[17] Minxiao Han, Hailong Wang, and Xiaojiang Guo, "Control Strategy Research of LCC Based Multi-terminal HVDC System," Proc. of IEEE International Conference on Power System Technology (POWERCON), pp. 1-5, Oct. 30-Nov. 2, 2012.

[18] Prabha Kundur, "Power System Stability and Control," McGraw-Hill, New York, 1994.

[19] J. P. Norton and B. J. Cory, "Control-system Stability in Multi-terminal HVDC Systems," Proc. IEE, vol. 115, no. 12, pp. 1828- 1834, Dec. 1968.

[20] K. R. Padiyar and Sachchidanand, "Stability of Converter Control for Multi-terminal HVDC System," IEEE Trans. Power Apparatus and Systems, vol. PAS-104, no. 3, pp. 690-696, Mar. 1985.

[21] N. Stao, N. V. Dravid, S. M. Chan, A. L. Burns, and J. J. Vithayathil, "Multiterminal HVDC System Representation in a Transient Stability Program," IEEE Trans. Power Apparatus and Systems, vol. PAS-99, no. 5, pp. 1927-1936, Sept. 1980.

[22] C. M. Ong and A. Hamzei-nejad, "Digital Simulation of Multiterminal HVDC Systems for Transient Stability Studies Using a Simplified DC System Representation," IEEE Trans. Power Apparatus and Systems, vol. PAS-104, no. 6, pp. 1411-1417, June 1985.

[23] P. K. Dash, M. A. Rahman, and P. C. Panda, "Dynamic Analysis of Power Systems with Multi-terminal HVDC Links and Static Compensators," IEEE Trans. Power Apparatus and Systems, vol. PAS-101, no. 6, pp. 1332-1341, June 1982.
[24] M. Szechtman, T. Wess, and C. V Thio, "A Benchmark Model for HVDC System Studies," Proc. of International Conference on AC and DC Power Transmission, pp. 374-378, Sep. 1991.
[25] M. Joorabian, S. Gh. Seifossadat, and M. A. Zamani, "An Algorithm to Design Harmonic Filters Based on Power Factor Correction for HVDC Systems," Proc. of IEEE International Conference on Industrial Technology, pp. 2978-2983, Dec. 2006.
[26] PSCAD/EMTDC User's Manual: Ver. 4.2, Manitoba HVDC Research Centre, 2005.
[27] J. P. Sucena-Paiva and L. L. Freris, "Stability of a DC Transmission Link between Strong AC Systems," Proc. IEE, vol. 120, no. 10, pp. 1233-1242, Oct. 1973.
[28] Simon S. Ang and Oliva Alejandro, "Power-Switching Converters," 2nd ed., Taylor & Francis, Inc., Mar. 2005, pp. 221-236.
[29] Farid Golnaraghi, and Benjamin C. Kuo, "Automatic Control System," 9th ed., Wiley, 2009, pp. 426-466.

Thai-Thanh Nguyen received his B.S degree in Electrical Engineering from Hanoi University of Science and Technology, Vietnam, in 2013. Currently, he is a combined Master and Ph. D. student in the Department of Electrical Engineering, Incheon National University, Korea. His research interests include power system analysis & modeling, FACTS, and HVDC.

Ho-Ik Son received his B.S degree in Electrical Engineering from Incheon National University, Korea, in 2012. Currently, he is a combined Master and Ph.D. student in the Department of Electrical Engineering, Incheon National University, Korea. His research interests include power system analysis & modeling, FACTS, and HVDC.

Hak-Man Kim received his first Ph. D. degree in Electrical Engineering from Sungkyunkwan University, Korea in 1998 and received his second Ph. D. degree in Information Sciences from Tohoku University, Japan, in 2011, respectively. He worked for Korea Electrotechnology Research Institute (KERI), Korea from Oct. 1996 to Feb. 2008. Currently, he is a professor in the Department of Electrical Engineering and also serves as the Vice Dean of College of Engineering, Incheon National University, Korea. His research interests include power system analysis & modeling, HVDC, FACTS, Microgrid, and LVDC.